NANO · MICRO small
www.small-journal.com

Microsphere-Based Nanoindentation for the Monitoring of Cellular Cortical Stiffness Regulated by MT1-MMP

Minhee Ku, Hyun-Joon Kim, Su Yee Yau, Nara Yoon, Nam Hee Kim, Jong In Yook, Jin-Suck Suh, Dae-Eun Kim, and Jaemoon Yang**

Biophysical properties are intimately connected to metastatic functions and aggressiveness in cancers. Especially, cellular stiffness is regarded as a biomarker for the understanding of metastatic potential and drug sensitivity. Here, protease-mediated changes of cortical stiffness are identified due to the deformation of cytoskeleton alignment at a cortex. For the past few decades, membrane type 1-matrix metalloproteinase (MT1-MMP) has been well known as a kernel protease enriched in podosomes during metastasis for extracellular matrix degradation. However, the biophysical significance of MT1-MMP expressing cancer cells is still unknown. Therefore, the nanomechanics of cancer cells is analyzed by a nanoindentation using a microsphere-attached cantilever of atomic force microscopy (AFM). In conclusion, the results suggest that MT1-MMP has contributed as a key regulator in cytoskeletal deformation related with cancer metastasis. Particularly, the AFM-based nanoindentation system for the monitoring of cortical nanomechanics will be crucial to understand molecular networks in cancers.

Cancer cells can alter the biophysical properties during a metastasis.[1–3] Several biomolecules related with the metastatic cascade have been discovered at the genetic/molecular level.[4,5] During tumor progression and metastasis, cancer cells increase the production of proteolytic enzymes, such as matrix metalloproteinases (MMPs) to detect extracellular cues and degrade the extracellular matrix.[6–9] Among various MMPs, membrane type 1-matrix metalloproteinase (MT1-MMP/MMP14) exhibit collagenolytic activities and functions in major developmental events.[10,11] Particularly, MT1-MMP can directly affect the early step of the metastatic cascade in primary tumors to alter their surrounding microenvironment during an invasion.[12–14] Migration and invasion of cancer cells have been extensively associated with MT1-MMP expression and activity.[15] Metastatic cancer cells have been mechanically softer than non-malignant cells, and the softness affects critical pathways and cellular processes for the cellular motility.[16–18] However, extensive studies are deficient to evaluate the role of MT1-MMP on the biophysical properties for cancer cells.

In this study, we thus have investigated the nanomechanical role of MT1-MMP expressed at cancer cells by the assessment of the cortical stiffness. Herein, atomic force microscopy (AFM) has been applied to analyze the nanomechanical properties of cancer cells and to understand their structural characteristics in the cortex.[19] AFM is one of the most effective techniques to measure the stiffness of a single

Dr. M. Ku, N. Yoon, Prof. J.-S. Suh, Prof. J. Yang
Department of Radiology
College of Medicine
Yonsei University
Seoul 03722, Republic of Korea
E-mail: 177hum@yuhs.ac

Dr. M. Ku, N. Yoon, Prof. J. Yang
Systems Molecular Radiology at Yonsei
Seoul 03722, Republic of Korea

Prof. H.-J. Kim
Department of Precision Mechanical Engineering
Kyungpook National University
2559, Gyeongsang-daero, Sangju 37224, Republic of Korea

S. Y. Yau, Prof. D.-E. Kim
Department of Mechanical Engineering
Yonsei University
Seoul 03722, Republic of Korea
E-mail: kimde@yonsei.ac.kr

The ORCID identification number(s) for the author(s) of this article can be found under https://doi.org/10.1002/smll.201803000.

S. Y. Yau, Prof. D.-E. Kim
Center of Nano-Wear
Yonsei University
Seoul 03722, Republic of Korea

Dr. N. H. Kim, Prof. J. I. Yook
Department of Oral Pathology
Oral cancer Research Institute
Yonsei University College of Dentistry
Seoul 03722, Republic of Korea

Prof. J.-S. Suh
YUHS-KRIBB Medical Convergence Research Institute
Seoul 03722, Republic of Korea

Prof. J.-S. Suh, Prof. J. Yang
Severance Biomedical Science Institute (SBSI)
Seoul 03722, Republic of Korea

Prof. J. Yang
Research Institute of Radiological Science
Yonsei University
Seoul 03722, Republic of Korea

DOI: 10.1002/smll.201803000

cell on the nanoscale because it uses various probe geometries (e.g., spherical, pyramidal, or conical probes) for the control over the loading and unloading position, force, and speed.[20] Thus, we have conducted microsphere-based nanoindentation for the monitoring of cellular cortical stiffness against cancer cells after the regulation of MT1-MMP. The expression level of MT1-MMP for the cancer cells was controlled by using siRNA (downregulation) and the tetracycline-dependent trans-activation (upregulation). To investigate the implication of MT1-MMP expression against the cortical stiffness, furthermore, cytoskeletal networks were sophisticatedly monitored by a confocal microscopy.

To investigate the relationship between cellular stiffness and the expression level of MT1-MMP, we respectively transfected human fibrosarcoma HT1080 cells with 10×10^{-9}, 25×10^{-9}, 50×10^{-9}, or 100×10^{-9} M of siMT1-MMP (**Figure 1**a). As a control, HT1080 cells were transfected with vehicle only (mock) and scrambled siRNA (siScr), respectively. To analyze the nanomechanics for the cortex of the transfected cancer cells, subsequently, the indentation experiment was performed using a microsphere-attached cantilever. As detailed depicted in Figure 1b, the diameter of the microsphere was selected in consideration of the cellular spreading. In several previous reports, diameter of the microsphere for cell indentation ranged from a few micrometers to ten micrometers.[21–23] However, we here utilized relatively large microsphere to avoid attainment of locally different stiffness owing to heterogeneous structure of the cell. Moreover, it was already reported that cellular stiffness depended on the indentation position.[24] In this work, since local distribution of the cellular stiffness was not a concern, relatively large microsphere was introduced to obtain representative characteristics of the concern cell. If large microsphere was exploited for the nanoindentation, relatively large area of the cell would be deformed during the process (Figure 1c,d). Therefore, the central part of the cell would be squeezed even the cantilever was misaligned. In addition, nondestructive deformation of the cell was expected when microspheres were applied compared to sharp tips. In this regard, the use of large microsphere may reduce marginal error in quantitative measurement. The spring constant of the cantilever is also an important parameter for determining the quality of the topological image depending on the type of specimen. When soft specimen was analyzed, compliant cantilever with low spring constant should be exploited to attain detectable signal through sufficient deflection of the cantilever as well as the specimen. Contrarily, stiff cantilever must be used for indentation experiment on a solid specimen to make cantilever comparably deform as the specimen. Several studies in which chose AFM cantilever where its spring constant was approximately a few N/m to investigate cell stiffness have been reported.[25–27] In this regard, relatively stiff cantilever was exploited to measure mechanical properties of fixed cell, which exhibited more stiff characteristics than living cell. Because the distance in the resulting force–distance (F–D) curves contained both the deformation of the cancer cell and the deflection of the cantilever, only the penetration depth, which represented the deformation of the cancer cell, was derived from the F–D curve; normal force relative to penetration depth was plotted (**Figure 2**a). The slope of a force-penetration depth curve corresponded to the stiffness of a cellular cortex and the steeper slope was seen in HT1080 cells transfected with siMT1-MMP than in control cells. To further explore the effect of MT1-MMP knockdown on cellular stiffness, the nanoindentation experiments on HT1080 cells transfected with 10×10^{-9}, 25×10^{-9}, 50×10^{-9}, or 100×10^{-9} M of siMT1-MMP were individually

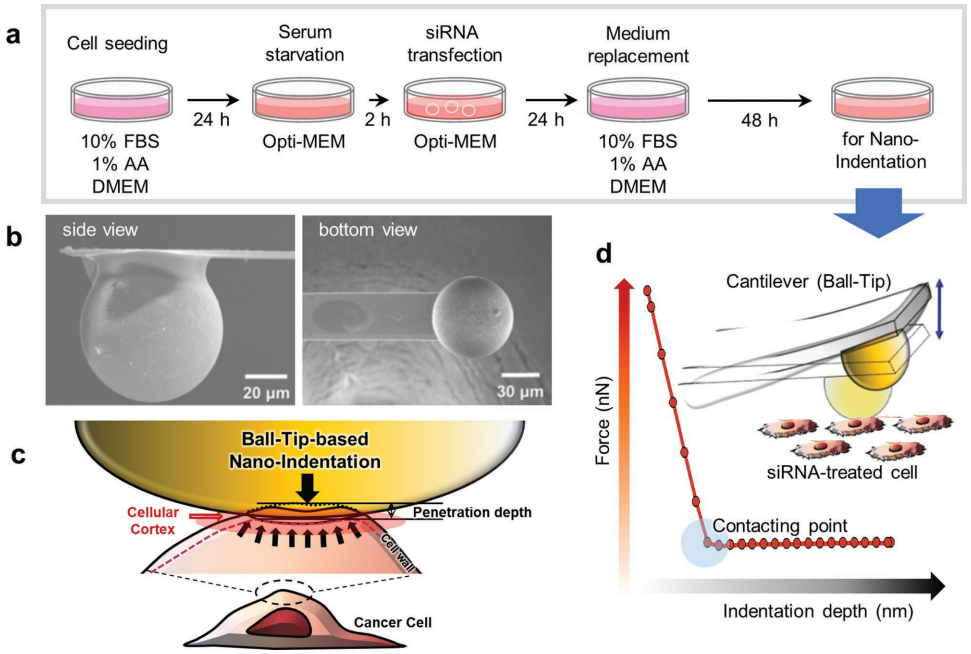

Figure 1. Schematics for the assessment of cellular cortical stiffness against MT1-MMP-regulated cancer cells. a) Process for the transfection of siMT1-MMP against cancer cells. b) Scanning electron microscope images for the AFM cantilever attached with a borosilicate glass microsphere (diameter: 62 μm); side view (left) and bottom view (right). c) Schematic illustration of the penetration depth resulting from the interaction of the ball tip and the cellular cortex that was applied for the calculation of the cellular stiffness. d) Schematics of force-indentation curve according to tip–sample interaction.

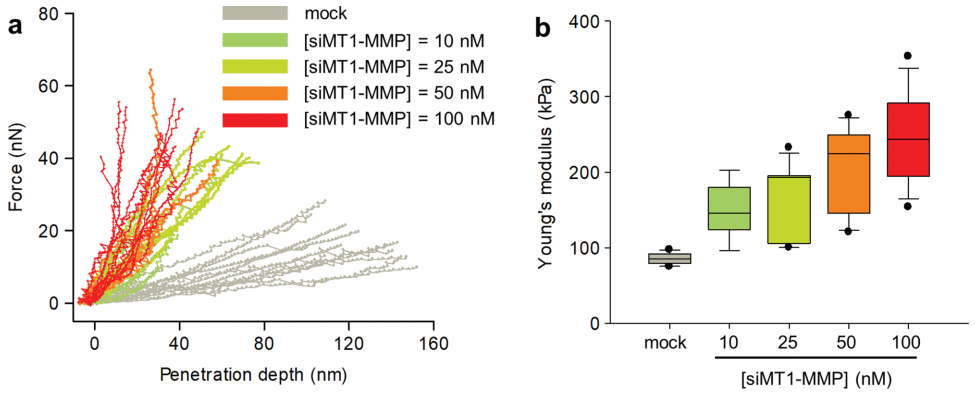

Figure 2. MT1-MMP regulates the cellular cortical stiffness of cancer cells. a) Graph for the relationship between force and penetration depth for HT1080 cells transfected with siMT1-MMP. b) Box plot of the Young's modulus of HT1080 cells transfected with siScr or various concentrations of siMT1-MMP. Box = the upper and lower quartiles, the short black line within a box = the median, and the circle = the outlier.

conducted (Figure S1a, Supporting Information). Cellular Young's modulus can be calculated from the force–indentation curve, the correction of the height for the cantilever bending to derive the tip-cell separation, by fitting them to the Hertz contact model.[28] Hertz model has been widely applied because of its simplicity for the analysis based on controlled measurement condition such as shallow indentation depth. We also measured the Young's modulus of cancer cells that were transfected with siScr or that were mock-transfected and found that the Young's modulus was not affected by transfection with siScr (Figure S1b, Supporting Information). Meanwhile, significant variations in cellular stiffness were found with varying siMT1-MMP concentrations (Figure 2b). The mock-transfected cells displayed low levels of stiffness (≈80–90 kPa). Even with significant deviations, the average Young's modulus of cells transfected with siMT1-MMP increased as the increase of siMT1-MMP concentration. The relatively high deviation was attributed to the fact that even though cells had similar properties, they exhibited complex dynamics under various conditions. To minimize error, tens of cells were examined for each condition of MT1-MMP and at least five times of indentation trials were conducted for each cell measurement. Then, the measured values were averaged. The average Young's modulus was 91 kPa for mock-transfected cells. The average Young's modulus was 149 kPa for HT1080 cells transfected with 10×10^{-9} M of siMT1-MMP, 162 kPa for cells transfected with 25×10^{-9} M of siMT1-MMP, 206 kPa for cells transfected with 50×10^{-9} M of siMT1-MMP, and 245 kPa for cells transfected with 100×10^{-9} M of siMT1-MMP. In fact, our measurement exhibited appropriate level of the Young's modulus ranged from 100 to 200 kPa reported by other research groups.[29–31] As a result, the cortical stiffness of the cancer cells was decreased as the increase of the expression of MT1-MMP. These data based on AFM-based nanoindentation demonstrate that MT1-MMP is a central organizer of cellular cortical stiffness.

To further delineate the relationship between reduced MT1-MMP expression and cellular cortical stiffness, MT1-MMP and cytoskeleton profiles for siScr-transfected and siMT1-MMP-transfected cancer cells were examined by an immunofluorescence confocal microscopy. siMT1-MMP-transfected cancer cells were immunostained with antibodies for filamentous actin (F-actin, red), nucleus (Hoechst 33342, blue), and MT1-MMP (Alexa488, green) (**Figure 3**a and Figure S2, Supporting Information). As expected, the fluorescent intensity

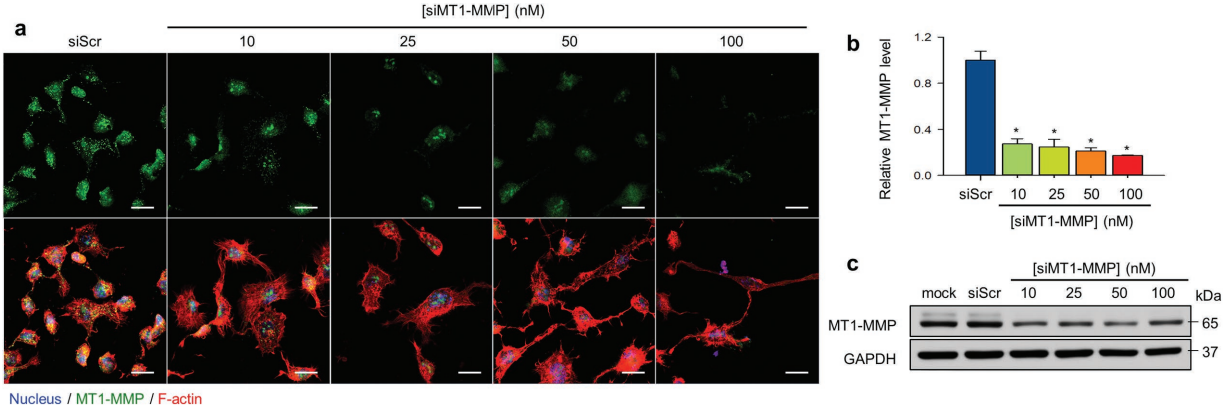

Figure 3. Downregulation of MT1-MMP leads to changes in cellular morphology. a) Confocal microscopic images of HT1080 cells transfected with siMT1-MMP; nucleus (blue), MT1-MMP (green), and F-actin (red). Scale bars: 20 µm. b) MT1-MMP mRNA expression levels measured by real-time PCR. Significant differences between the siScr group and all of the other groups were observed (*$p < 0.01$). c) MT1-MMP protein expression levels in HT1080 cells that were transfected with siMT1-MMP were analyzed by Western blot. Full-length blots are presented in Figure S3 in the Supporting Information.

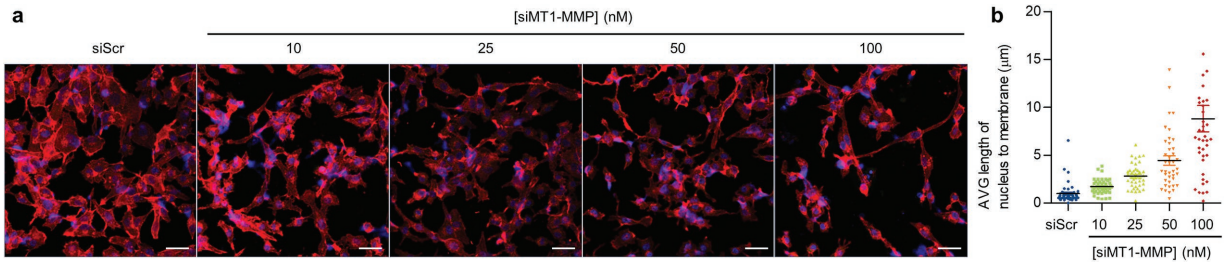

Figure 4. a) Maximal projection confocal microscopic images of HT1080 cells transfected with siMT1-MMP; nucleus (blue) and F-actin (red). Scale bars: 20 μm. b) Dot plot for the length from the nucleus to the membrane of HT1080 cells ($n > 40$) transfected with siMT1-MMP from (a). Black line: average length.

from MT1-MMP of the cells was decreased as the increase of siMT1-MMP concentration. By 3D-reconstruction confocal microscopy, moreover, the differences in MT1-MMP expression in siScr-transfected and siMT1-MMP-transfected cells could be confirmed (Video S1, Supporting Information). Subsequently, MT1-MMP expression levels in siScr- and siMT1-MMP-transfected cells were investigated by real-time polymerase chain reaction (PCR) and Western blot. After the transfection, MT1-MMP mRNA levels were lower in siMT1-MMP-treated cells compared to siScr-transfected cells (Figure 3b). Moreover, a reduction in MT1-MMP protein (64 kD) expression in siMT1-MMP-transfected cells was confirmed by Western blot (Figure 3c and Figure S3, Supporting Information).

In contrast to siScr-transfected cells, on the other hand, siMT1-MMP-transfected cells exhibited morphological changes from F-actin staining. We thus quantified the cellular deformability in siMT1-MMP-transfected cells by the maximal projection images from confocal microscopy (**Figure 4**a). The average protrusion length from the nucleus to the membrane along the longest major axis was measured for over 40 randomly selected cells. In Figure 4b, the results demonstrated that siMT1-MMP-transfected cells exhibited longer protrusion length from the nucleus to the membrane compared to siScr-transfected cells. The protrusion length of cells transfected with 100×10^{-9} M of siMT1-MMP was ≈8.82-fold larger than the siScr-transfected cells. The results presented that the downregulation of MT1-MMP might increase cellular deformability. In order to confirm the effect on MT1-MMP-mediated motility, in addition, real-time monitoring of the interrogated single was conducted. Using a time-lapse microscopy, siScr- and siMT1-MMP-transfected cells were respectively monitored for discovering cellular behaviors of single cell. Cell movement images indicated that changes in cell shape were contributed to the migration activity of cells. In support of this, the depletion of MT1-MMP promoted multipolar cell morphology and induces motility arrest (Video S2, Supporting Information). In particular, siScr-transfected cells exhibited flatly spreading and siMT1-MMP-transfected cells exhibited multipolar stretching. In recent report, morphological characteristics of cancer cells are essential for determining cell shape, structure, size, and functional properties.[32] The correlation graph between morphological deformation and the variation of Young's modulus of cells according to MT1-MMP expression was investigated (**Figure 5**). Finally, we found that knockdown of MT1-MMP had affected the Young's modulus at the cortex and cellular morphology.

As previous results, we have found the differences in cellular stiffness for MT1-MMP-regulated cancer cells. Thus, we have inferred that MT1-MMP-mediated change for cytoskeletal F-actin networks might be a key determinant of the shape and mechanical behavior of the interesting cell.[3] According to z-stack confocal microscopic images, the *z*-axis height of the cell ranged from 4.48 to 5.6 μm and the penetration depth ranged from 0.04 to 0.15 μm, which indicated cellular deformation as a result of contact with a microsphere attached to an AFM cantilever that detected cellular stiffness and F-actin distribution in the cellular cortex. As a result of confocal microscopic image, the F-actin bundles were uniformly aligned along the lamellipodia and filopodia of the cells in siScr-transfected HT1080 cells (**Figure 6**a,b). In contrast, siMT1-MMP-transfected HT1080 cells had disrupted F-actin bundles and expressed spot-like patterns (Figure 6d,e). In addition, the fluorescence intensity maps obtained from F-actin staining demonstrated the change of cytoskeletal network after the transfection of siMT1-MMP (Figure 6c,f). Herein, changes in cell morphology might be attributed to redistribution of the actin network, which transformed cellular stiffness and single cell spreading. Invasive tumor cells have been shown to exhibit a lower mean stiffness relative to noncancerous cells and stiffness correlated

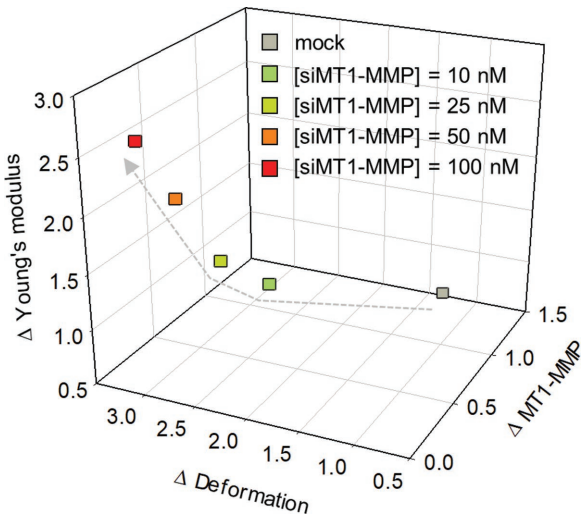

Figure 5. 3D-correlative graph of the relationship between relative MT1-MMP mRNA expression, relative cellular deformation, and relative Young's modulus. MT1-MMP expression affects cellular deformation and the relative Young's modulus (gray dotted arrow).

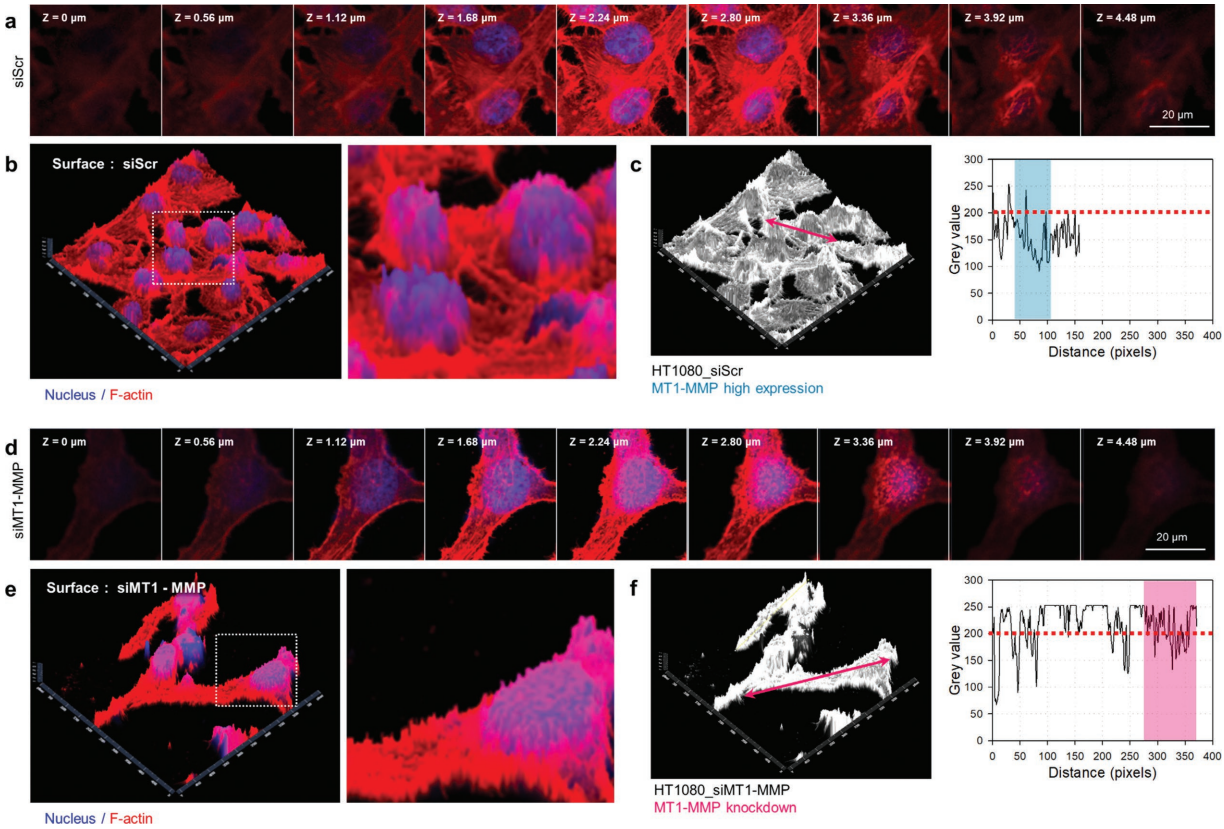

Figure 6. Change of F-actin-based cytoskeletal network at cellular cortex by MT1-MMP regulation. Sequential confocal microscopy of HT1080 cells transfected with a) siScr or d) siMT1-MMP along *z*-axis; blue is nucleus and red is F-actin. The slice thickness (Δz) is 0.56 μm. b,e) 3D-stacked confocal microscopic image and its magnificated image from (a) and (e), respectively. The magnificated images obtained from white dotted boxed. The change of cortical F-actin networks was observed after the regulation of MT1-MMP. c,f) The fluorescence intensity map images and gray value graphs based on the red arrow lines. Red dotted lines mean 200 gray value.

with malignancy and malignant gene expression.[33,34] In addition, each phase of the metastatic process requires a specific molecular biomarker that regulates the actin-based protrusions.[35–38] Considering the interaction between ball tip and cells, these changes in the alignment of F-actin bundles served as an important parameter for determining cortical stiffness. Therefore, siMT1-MMP had induced cellar morphological deformation and the change of actin-based cytoskeletal network related with cortex thickness and density.

On the other hand, we extensively investigated the role of MT1-MMP in MT1-MMP-deficient cancer cells. MCF7 cells, as a breast cancer cell line, with low expression levels of MT1-MMP were mainly used as a control cell for MT1-MMP-related experiments.[39] Thus, we examined the effects of MT1-MMP expression on the morphology and cortical stiffness of MCF7 cells. Using a doxycycline-dependent MT1-MMP-inducible vector based on Tet-On system, MCF7 cells were cultured in the absence or presence of 5 μg mL^{-1} of doxycycline for 48 h. The expression level of MT1-MMP was determined by immunofluorescence staining in wild-type MCF7 cells ($MCF7^{WT}$) and MT1-MMP-upregulated ($MCF7^{MT1+}$) (**Figure 7**a). $MCF7^{MT1+}$ cells exhibited decreased multipolarized structure of protrusion and increased motility compared to $MCF7^{WT}$ cells (Figure 7b). After the induction of MT1-MMP, in particular, lamellipodium was observed (red arrows from Figure 7b). These results were considered to reflect the effect of membrane protrusion and invasive potential by MT1-MMP activity.[40] After the strict reconstitution of cellular network, we separated the lines from the images and displayed them in geometric patterns and graphs for the length of the edges (internuclear distance) and distribution area constituting the network. Interestingly, MT1-MMP-expressing $MCF7^{MT1+}$ cells presented more disorganized spatial distribution compared to control $MCF7^{WT}$ cells (Figure 7c). $MCF7^{MT1+}$ cells exhibited increased internuclear distance (36.30 ± 9.98 μm) and distribution area (139.35 ± 71.74 μm) compared to $MCF7^{WT}$ cells (internuclear distance = 18.55 ± 6.65 μm and distribution area = 71.50 ± 52.14 μm). Subsequently, we have assessed the cortical stiffness for MT1-MMP-induced MCF7 cells (Figure 7d). As presented in the force–distance curve, $MCF7^{MT1+}$ cells represented a significant decrease in the force per penetration depth compared to $MCF7^{WT}$ cells. In particular, cellular Young's modulus for $MCF7^{MT1+}$ cells was remarkably reduced after the induction of MT1-MMP (Figure 7e). As shown in **Figure 8**a,b,d,e, on the other hand, z-stack and 3D-reconstructed confocal microscopic images demonstrated the changes of F-actin-based cytoskeletal network due to the induction of MT1-MMP. In case of $MCF7^{WT}$ cells, stretched cortical actin networks surrounding nucleus were observed. In contrast, $MCF7^{MT1+}$ cells had lamellipodium to one side and thinned cortex. The difference in the cortical

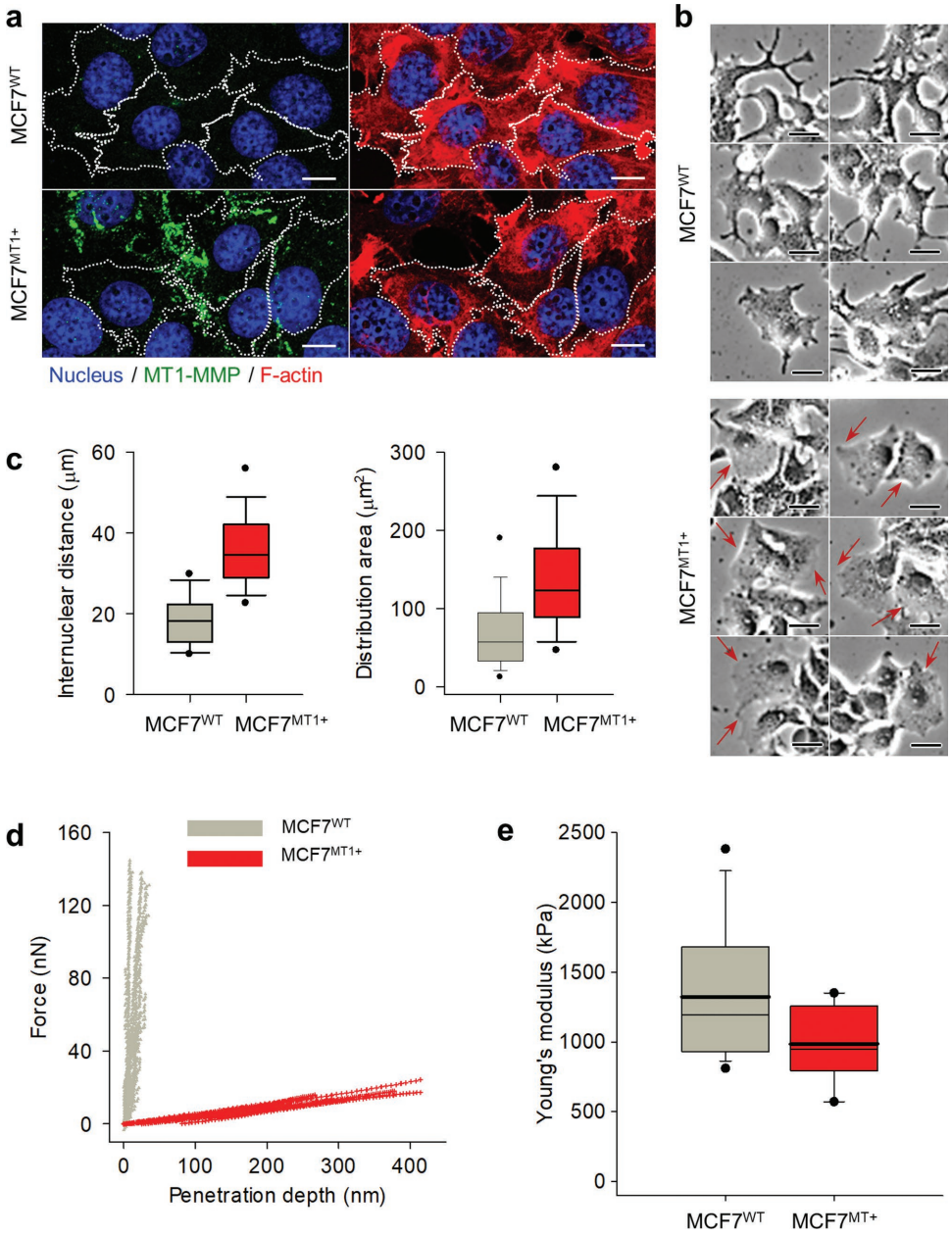

Figure 7. Cellular morphological change in MT1-MMP-induced MCF7 cells. a) Confocal microscopic images of wild type ($MCF7^{WT}$) and MT1-MMP-induced MCF7 cells ($MCF7^{MT1+}$); nucleus (blue), MT1-MMP (green), and F-actin (red). Scale bars: 10 μm. b) Phase microscopic images depicted cell morphology of $MCF7^{WT}$ and $MCF7^{MT1+}$ cells. Scale bars: 20 μm. Red arrows mean spreading sites of cells. c) Box plots of internuclear distance and distribution area relative to the quantification from the cellular networks. Box = the upper and lower quartiles, the short black line within a box = the median, and the circle = the outlier. d) Graph for the relationship between force and penetration depth for $MCF7^{WT}$ (gray) and $MCF7^{MT1+}$ (red) cells. e) Box plots of the Young's modulus of $MCF7^{WT}$ (gray) and $MCF7^{MT1+}$ (red) cells. Box = the upper and lower quartiles, the thin black line within a box = the median, the thick black line within a box = mean, and the circle = the outlier.

stiffness could be inferred from changes in F-actin networking (Figure 8c,f). These results demonstrated that MT1-MMP-upregulated cancer cells exhibited weaker cell–cell network and spreading morphology. In particular, the cortical stiffness of the cancer cells was controlled by the expression of MT1-MMP.

We here demonstrated that the microsphere-based nanoindentation was enable to monitor the cellular cortical stiffness after the modulation of the specific molecule expression for cancer cells. In especial, MT1-MMP expression modulated cellular nanomechanical characteristics of cancer cells by the reorganization of F-actin-based cytoskeletal network. Importantly, we here suggest the novel role of MT1-MMP as a kernel controller in the cellular cortical mechanics. Furthermore, these results also provide a predictable parameter of cancer cell behavior, suggesting that a strong association between MT1-MMP and F-actin networking may orchestrate the mechanisms underlying

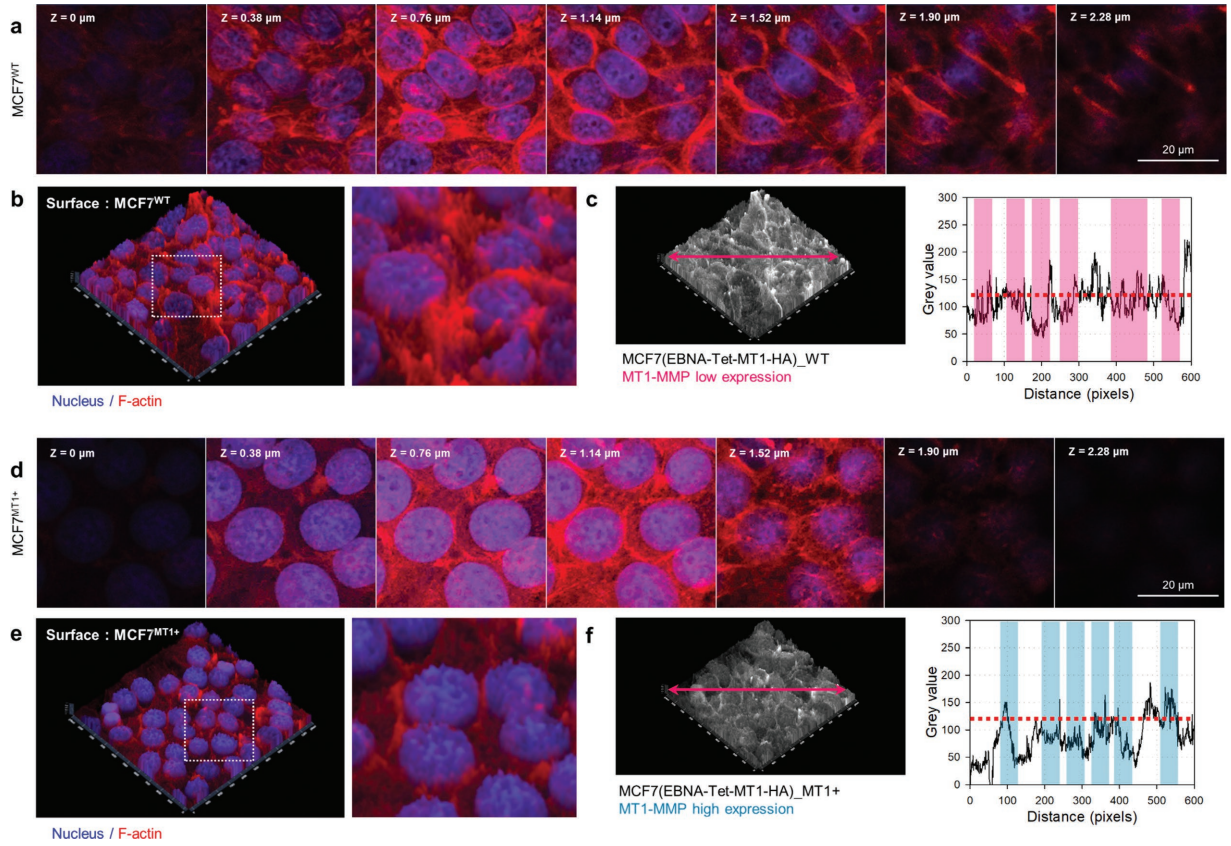

Figure 8. Change of F-actin-based cytoskeletal network at cellular cortex by MT1-MMP regulation. Sequential confocal microscopy of MCF7 cells transfected with a) $MCF7^{WT}$ or d) $MCF7^{MT1+}$ along *z*-axis; blue is nucleus and red is F-actin. The slice thickness (Δz) is 0.38 μm. b,e) 3D-stacked confocal microscopic image and its magnificated image from (a) and (e), respectively. The magnificated images obtained from white dotted boxed. The change of cortical F-actin networks was observed after the regulation of MT1-MMP. c,f) The fluorescence intensity map images and gray value graphs based on the red arrow lines. Red dotted lines mean 120 gray value.

the metastatic behaviors of cancer cells. These findings are consistent with a previous study for MT1-MMP activation correlated with the metastatic properties and spreading patterns of cancer cells.[41] Hence, the AFM-based nanomechanical insights using Hertz model will advance our understanding of cancer progression and provide a tool in screening an effective anticancer drug with the help of biochemical signatures.

Experimental Section

Cell Culture: The human fibrosarcoma cell line HT1080 was obtained from the American Type Culture Collection (Manassas, VA, USA) and cultured in minimum essential medium (MEM) (Gibco, Carlsbad, CA, USA) medium supplemented with 10% fetal bovine serum (FBS) (Gibco) at 37 °C in a 5% CO_2 humidified atmosphere. Human breast cancer cell line, MCF7 cells were obtained from the Korean Cell Line Bank (Korean Cell Line Research Foundation, Seoul, Korea) and cultured in RPMI1640 (Gibco) medium supplemented with 10% FBS. The tetracycline-dependent trans-activated MCF7 cell lines (doxycycline-inducible expression of tagged hemagglutinin (HA) or MT1-MMP, Epstein-Barr virus nuclear antigen (EBNA)-Tet-MT1-HA) cells were cultured in Dulbecco modified Eagle medium (Gibco) medium with 10% [-] Tetracycline FBS (Gibco) with doxycycline 5 μg mL^{-1} for 48 h for MT1-MMP expression. Doxycycline hyclate (Sigma-Aldrich, St. Louis, MO, USA) was dissolved in deionized water at 5 mg mL^{-1} for storage and diluted with growth medium to a working concentration.

siRNA Transfection: HT1080 cells were plated at 2×10^5 cells per well in six-well dishes and 1×10^4 cells per well in E-plate 16 devices (ACEA Biosciences, San Diego, CA, USA). When cells reached 70–80% confluence, they were transfected using Lipofectamine 2000 (Life Technologies, Inc., Gaithersburg, MD, USA) transfection reagent according to the manufacturer's protocol. siRNA oligonucleotides for MT1-MMP (siMT1-MMP) were synthesized by Bioneer (Daejeon, Korea) and a nontargeting scrambled siRNA (siScr) was used as a negative control. The siMT1-MMP sequences were 5′-CAG GCA AAG CUG AUG CAG AUU (dTdT)-3′ and 3′-(dTdT) AAU CUG CAU CAG CUU UGC CUG-5′.[42–44] The cells were transfected with 10×10^{-9}, 25×10^{-9}, 50×10^{-9}, or 100×10^{-9} M of siRNA for 24 h using Lipofectamine 2000 and Opti-MEM (Gibco, Carlsbad, CA, USA) medium following the manufacturer's protocol (Thermo Scientific, Waltham, MA, USA).

RNA Isolation and cDNA Synthesis: HT1080 cells were harvested for RNA isolation 24 h after transfection with siMT1-MMP. Total RNA was extracted using the Ambion mirVana miRNA Isolation Kit (Ambion, Austin, TX, USA) and the quality of the isolated RNA was evaluated using a NanoDrop Lite Spectrophotometer (Thermo Scientific, Wilmington, MA, USA).[44] All of the samples had a 260/280 ratio of ≈2.0. Total RNA was converted to cDNA using a high capacity RNA-to-cDNA kit (Applied Biosystems, Carlsbad, CA, USA) according to the manufacturer's recommendation.

Quantitative Real-Time PCR: cDNA synthesis using 1 μg of RNA per 20 μL of reaction was performed using the Roche LightCycler system (Roche Diagnostics). Quantitative real-time PCR was performed in triplicate using HiFast SYBR Lo-Rox reagents (GenePole, Edinburgh, UK). Thermocycling conditions were as follows: initial denaturation at

95 °C for 10 min followed by 45 cycles at 95 °C for 10 s (annealing) and 60 °C for 30 s (extension). Primer sequences were designed using Primer3 software (http://frodo.wi.mit.edu/primer3/) and included MT1-MMP (forward: 5′-TCT ATG GCG CTG AGA TTG TG-3′, reverse: 5′-CTT AAT GTG CCC GTC CTT GT-3′) and β-actin (forward: 5′-CTC TTC CAG CCT TCC TTC CT-3′, reverse: 5′-TGT TGG CGT ACA GGT CTT TG-3′).[45] The $2^{-\Delta\Delta Ct}$ method was used to calculate fold differences in gene expression and the β-actin gene was used as the housekeeping reference for data normalization. The PCR products were subjected to melting curve analyses to rule out synthesis of nonspecific products.

Western Blotting: Total protein from HT1080 cells was extracted by treating the cells with radioimmunoprecipitation assay buffer (Cell Signaling Technology, Danvers, MA, USA) for 20 min at 4 °C, and then samples were centrifuged for 10 min at 15 700 g. Protein concentrations were determined by bicinchoninic acid (BCA) assay (BCA protein assay reagent A and B, Pierce Biotechnology, Rockford, IL, USA). For each sample, 15 µg of protein was electrophoresed through a 10% sodium dodecyl sulfate-polyacrylamide gel and transferred to a polyvinylidene fluoride membrane for 2 h at 4 °C. Each membrane was blocked for 1 h at room temperature with blocking buffer (5% skim milk in 1 × tris-buffered saline with Tween-20) and then incubated overnight at 4 °C with a 1:1000 dilution of primary antibody. The primary antibodies included anti-MT1-MMP (Abcam Inc., Cambridge, MA, USA) and anti-glyceraldehyde 3-phosphate dehydrogenase (Santa Cruz Biotechnology, Dallas, TX, USA). Primary antibody binding was detected with horseradish peroxidase (HRP)-labeled secondary antibody and Immobilon Western chemiluminescent HRP substrate enhanced chemiluminescence solution (Merck Millipore, Darmstadt, Germany) using a luminescent image analyzer (LAS-4000, GE Healthcare Life Sciences, Pittsburgh, PA, USA).

Immunofluorescence Confocal Microscopy: siScr or siMT1-MMP-transfected HT1080 and WT or MT1-MMP-induced MCF7 cells were plated on coverslips at a cell density of 5×10^4 in a flat-bottom four-well plate. The cells were then fixed for 30 min in 1 × phosphate buffered saline (PBS) supplemented with 4% formaldehyde. Subsequently, the cells were washed three times with PBS and then permeabilized with 0.5% Triton X-100 in PBS for 15 min. The cells were washed three times with PBS contained 0.1% bovine serum albumin and incubated for 30 min for blocking. The cells were incubated for 30 min at 22 °C with primary antibody diluted 1:200. The cells were then washed three times and incubated with a 1:500 dilution of secondary antibody for 30 min at 22 °C. Finally, the cells were washed three more times with PBS. Ten minutes before analyzing the plate, a nucleus staining solution-containing Hoechst33342 (Molecular Probes, Waltham, MA, USA) was added to a final concentration of 5 mg mL^{-1}. Microscopic images were captured using a confocal microscope (LSM-700, Carl Zeiss, Jena, Germany) with a 63 × objective and ZEN software (version 5.5.0.375, Carl Zeiss), which was designed for the acquisition and processing of confocal microscope images. Computerized pseudo colors were added to differentiate the various fluorescence channels and to generate the final colored images. The cellular deformation ratio was calculated by selecting the cellular boundary and measuring the mean pixel intensity inside the defined area using ImageJ.

Cell Migration Assay: For the cell migration assay, migration of HT1080 cells that were transfected with siScr or 100×10^{-9} M of siMT1-MMP and MCF7 (EBNA-Tet-MT1-HA) cells that were MT1-MMP transaction with doxycycline were observed for 200 min using the live image movie analyzer (JuLI Br, NanoEnTeck, Pleasanton, CA, USA). The movie was made using 20 images captured at 10 min intervals to quantify the number of cells.

Real-Time Cell Analyzer Cell Invasion Assay: Cell invasion was analyzed using the xCELLigence DP system (Roche Diagnostics GmbH, Berlin, Germany). To monitor cell indices, HT1080 cells that were transfected with siScr or siMT1-MMP and MCF7(EBNA-Tet-MT1-HA) cells that were MT1-MMP transaction with doxycycline were seeded at a density of 4×10^4 cells per well in the upper chambers of cell invasion/migration (CIM) plates (ACEA Biosciences, San Diego, CA, USA) containing serum-free culture medium. The upper chambers were coated with 30 µL of a 1:20 dilution of Matrigel (BD Bioscience, Bedford, MA, USA) to create a 3D biomatrix film in each well prior to cell loading. The upper chamber was then placed in the lower part of the CIM plate containing growth medium supplemented with 10% FBS to promote invasion across the membrane and toward the serum gradient. Cell invasion was monitored for 24 h by measuring changes in the impedance signal in the CIM plate on the opposite side of the membrane. Impedance data were collected at 1 h intervals for ≈25 h and expressed as CI (cell index) values. To calculate the CI, the formula $CI = (Z_i - Z_0)/15\varsigma$, in which Z_i is the impedance at an individual time point during the experiment and Z_0 is the impedance at the start of the experiment, was used. Cell adherence data were normalized 24 h after seeding. The normalized CI is calculated by dividing the CI at the normalized time by the original CI. For each condition, experiments were performed in triplicate and data were expressed as average ± standard deviation.

Cell Morphology and Directional Migratory Studies: HT1080 cells that were transfected with siScr or 100×10^{-9} M of siMT1-MMP and MCF7 (EBNA-Tet-MT1-HA) cells that were MT1-MMP transaction with doxycycline were seeded into six-well plates at 1×10^5 cells per well. Cells were monitored with Cell-IQ (Chip-man Technologies Oy, Tampere, Finland) for dynamic phase contrast imaging in a humidified 5% CO_2 atmosphere at 37 °C. Images were captured automatically from six positions per well at 10 min intervals for 8 d. A protocol for quantifying cell numbers with Cell-IQ analyzer software was created according to manufacturer's instructions.

Nanoindentation Assay: The indentation experiment was conducted using an AFM (Seiko Instruments Inc., Chiba, Japan). For the measurement of the Young's modulus of cancer cells, a relatively long AFM cantilever with a spring constant of 0.48 N m^{-1} was chosen. Length and width of the cantilever used in this study were 430 and 52 µm, respectively. The spring constant of the cantilever was determined by measuring the geometry and resonant characteristics of the cantilever in accordance with the Sader method.[46] A borosilicate glass microsphere (diameter = 62 µm) was attached to the end of the cantilever to better assess cell elasticity by examining a larger area. To obtain accurate measurements, the cantilever was positioned to carefully indent the center of the cancer cell. The indentation speed was set to ≈40 nm s^{-1} and the indentation depth was set to less than 200 nm to avoid destroying the cell. In addition, it is generally accepted that 10% of indentation depth to the thickness of the target material can give consistent result regardless of substrate effect.[47–49] Therefore, indentation depth was controlled to be less than 200 nm to eliminate influence of the substrate or cell height. For accurate quantification, each cell was indented over ten times and the resulting values were averaged.

Calculation of the Young's Modulus: For assessment of cancer cell stiffness, the Young's modulus of a cell was calculated using the Hertz contact model as shown in Equation (1)

$$E = \frac{3}{4}\frac{(1-\nu^2)}{\sqrt{R}}\frac{dF}{d(p^{3/2})} \quad (1)$$

in which E represents the Young's modulus, F represents the normal force during indentation, ν represents the Poisson's ratio, R represents the radius of the sphere, and p represents the deformation of the cancer cell.[50] Because it is generally accepted that the Poisson's ratio for cells and tissue is 0.5, this value was used for the Poisson's ratio. The Hertz contact model is based on two assumptions. One assumption is that the indenter shape has to be parabolic and the other is that the thickness of the sample to be indented must be significantly thicker than the indentation depth.[51] These assumptions were satisfied because the indenter used was a glass sphere with a diameter that was significantly larger than the cancer cell, and the indentation depth was below 200 nm and was estimated to be ten times smaller than the height of the cancer cell. Hence, the application of the Hertz contact model in this work was adequate.

Statistical Analysis: The in vitro results were expressed as mean ± standard deviation. The student's t-test was performed to determine significant differences between groups and p-values <0.01 or <0.05 were considered significant.

Supporting Information

Supporting Information is available from the Wiley Online Library or from the author.

Acknowledgements

This work was supported by the National Research Foundation (NRF) grants (2017R1C1B2010867, 2014R1A1A2059806, and 2015R1A2A1A05001887) funded by the Ministry of Science, ICT and Future Planning (MSIP) and the National Research Foundation of Korea (NRF) grant funded by the Korea government(MSIT) (2010-0018289). This work was also supported by a grant from the National R&D Program for Cancer Control (1220100) and the Korea Health Technology R&D Project through the Korea Health Industry Development Institute (HI17C2586), funded by the Ministry of Health and Welfare, Republic of Korea.

Conflict of Interest

The authors declare no conflict of interest.

Keywords

atomic force microscopy, cancer mechanobiology, cortical stiffness, MT1-MMP, nanoindentation

Received: July 30, 2018
Revised: August 21, 2018
Published online:

[1] D. Wirtz, K. Konstantopoulos, P. C. Searson, *Nat. Rev. Cancer* **2011**, *11*, 512.
[2] C. Denais, J. Lammerding, *Adv. Exp. Med. Biol.* **2014**, *773*, 435.
[3] W. Xu, R. Mezencev, B. Kim, L. Wang, J. McDonald, T. Sulchek, *PLoS One* **2012**, *7*, e46609.
[4] F. C. Bidard, J. Y. Pierga, J. C. Soria, J. P. Thiery, *Nat. Rev. Clin. Oncol.* **2013**, *10*, 169.
[5] J. Fenner, A. C. Stacer, F. Winterroth, T. D. Johnson, K. E. Luker, G. D. Luker, *Sci. Rep.* **2015**, *4*, 5512.
[6] P. Cai, M. Layani, W. R. Leow, S. Amini, Z. Liu, D. Qi, B. Hu, Y. L. Wu, A. Miserez, S. Magdassi, X. Chen, *Adv. Mater.* **2016**, *28*, 3102.
[7] M. Egeblad, Z. Werb, *Nat. Rev. Cancer* **2002**, *2*, 161.
[8] C. Gialeli, A. D. Theocharis, N. K. Karamanos, *FEBS J.* **2011**, *278*, 16.
[9] A. Das, M. Monteiro, A. Barai, S. Kumar, S. Sen, *Sci. Rep.* **2017**, *7*, 14219.
[10] A. R. Folgueras, A. M. Pendás, L. M. Sánchez, C. López-Otín, *Int. J. Dev. Biol.* **2004**, *48*, 411.
[11] J. Ueda, M. Kajita, N. Suenaga, K. Fujii, M. Seiki, *Oncogene* **2003**, *22*, 8716.
[12] J. Y. Perentes, N. D. Kirkpatrick, S. Nagano, E. Y. Smith, C. M. Shaver, D. Sgroi, I. Garkavtsev, L. L. Munn, R. K. Jain, Y. Boucher, *Cancer Res.* **2011**, *71*, 4527.
[13] K. Wolf, Y. Wu, Y. Liu, J. Geiger, E. Tam, C. Overall, M. S. Stack, P. Friedl, *Nat. Cell Biol.* **2007**, *9*, 893.
[14] B. Hu, W. R. Leow, S. Amini, B. Nai, X. Zhang, Z. Liu, P. Cai, Z. Li, Y. L. Wu, A. Miserez, C. T. Lim, X. Chen, *Adv. Mater.* **2017**, *29*, 1700145.
[15] E. I. Deryugina, J. P. Quigley, *Cancer Metastasis Rev.* **2006**, *25*, 9.
[16] T. Hasegawa, K. Yamakado, A. Nakatsuka, J. Uraki, T. Yamanaka, M. Fujimori, M. Miki, T. Sasaki, H. Sakuma, Y. Sugimura, *Radiology* **2015**, *277*, 584.
[17] D. S. Lee, Y. S. Kim, C. S. Kay, S. H. Kim, C. D. Yeo, J. W. Kim, S. J. Kim, Y. K. Kim, Y. H. Ko, J. H. Kang, K. Y. Lee, *Medicine* **2016**, *95*, e2795.
[18] B. Hu, W. Shi, Y. L. Wu, W. R. Leow, P. Cai, S. Li, X. Chen, *Adv. Mater.* **2014**, *26*, 5786.
[19] K. D. Costa, *Dis. Markers* **2004**, *19*, 139.
[20] E. Y. Kwon, Y. T. Kim, D. E. Kim, *J. Mech. Sci. Technol.* **2009**, *23*, 1932.
[21] M. Lekka, *Bionanoscience* **2016**, *6*, 65.
[22] Y. M. Efremov, A. A. Dokrunova, A. V. Efremenko, M. P. Kirpichnikov, K. V. Shaitan, O. S. Sokolova, *Biochim. Biophys. Acta, Mol. Cell Res.* **2015**, *1853*, 3117.
[23] M. Nikkhah, J. S. Strobl, E. M. Schmelz, M. Agah, *J. Biomech.* **2011**, *44*, 762.
[24] J. Rheinlaender, N. A. Geisse, R. Proksch, T. E. Schäffer, *Langmuir* **2011**, *27*, 697.
[25] G. E. Yakubov, M. R. Bonilla, H. Chen, M. S. Doblin, A. Bacic, M. J. Gidley, J. R. Stokes, *J. Exp. Bot.* **2016**, *67*, 2799.
[26] L. Ramms, G. Fabris, R. Windoffer, N. Schwarz, R. Springer, C. Zhou, J. Lazar, S. Stiefel, N. Hersch, U. Schnakenberg, T. M. Magin, R. E. Leube, R. Merkel, B. Hoffmann, *Proc. Natl. Acad. Sci. USA* **2013**, *110*, 18513.
[27] H. Ladjal, J. L. Hanus, A. Pillarisetti, C. Keefer, A. Ferreira, J. P. Desai, presented at *Proc. IEEE/RSJ Int. Conf. Intell. Robot. Syst.*, St. Louis, October, **2009**.
[28] D. C. Lin, E. K. Dimitriadis, F. Horkay, *J. Biomech. Eng.* **2007**, *129*, 430.
[29] J. Seifert, J. Rheinlaender, P. Novak, Y. E. Korchev, T. E. Schäffer, *Langmuir* **2015**, *31*, 6807.
[30] A. Pillarisetti, C. Keefer, J. P. Desai, in *Experimental Robotics: The Eleventh International Symposium*, Vol. *54* (Eds: O. Khatib, V. Kumar, G. J. Pappas), Springer, Heidelberg, Germany **2009**, Sess. 6.
[31] F. Braet, C. Rotsch, E. Wisse, M. Radmacher, *Appl. Phys. A: Mater. Sci. Process.* **1998**, *66*, S575.
[32] S. M. Lyons, E. Alizadeh, J. Mannheimer, K. Schuamberg, J. Castle, B. Schroder, P. Turk, D. Thamm, A. Prasad, *Biol. Open* **2016**, *5*, 289.
[33] J. R. Staunton, B. L. Doss, S. Lindsay, R. Ros, *Sci. Rep.* **2016**, *6*, 19686.
[34] V. Palmieri, D. Lucchetti, A. Maiorana, M. Papi, G. Maulucci, F. Calapà, G. Ciasca, R. Giordano, A. Sgambato, M. De Spirito, *Soft Matter* **2015**, *11*, 5719.
[35] H. Paz, N. Pathak, J. Yang, *Oncogene* **2014**, *33*, 4193.
[36] F. J. Sulzmaier, C. Jean, D. D. Schlaepfer, *Nat. Rev. Cancer* **2014**, *14*, 598.
[37] X. Guan, *Acta Pharm. Sin. B* **2015**, *5*, 402.
[38] C. T. Mierke, P. Kollmannsberger, D. P. Zitterbart, G. Diez, T. M. Koch, S. Marg, W. H. Ziegler, W. H. Goldmann, B. Fabry, *J. Biol. Chem.* **2010**, *285*, 13121.
[39] M. Ku, Y. Hong, D. Heo, E. Lee, S. Hwang, J. S. Suh, J. Yang, *Biosens. Bioelectron.* **2016**, *77*, 471.
[40] C. Chevalier, G. Collin, S. Descamps, H. Touaitahuata, V. Simon, N. Reymond, L. Fernandez, P. E. Milhiet, V. Georget, S. Urbach, L. Lasorsa, B. Orsetti, F. Boissière-Michot, E. Lopez-Crapez, C. Theillet, S. Roche, C. Benistant, *Nat. Commun.* **2016**, *7*, 10765.
[41] M. Kajita, Y. Itoh, T. Chiba, H. Mori, A. Okada, H. Kinoh, M. Seiki, *J. Cell Biol.* **2001**, *153*, 893.
[42] X. Y. Li, I. Ota, I. Yana, F. Sabeh, S. J. Weiss, *Mol. Biol. Cell* **2008**, *19*, 3221.
[43] H. C. Lim, H. A. Multhaupt, J. R. Couchman, *Mol. Cancer* **2015**, *14*, 15.
[44] P. Mamidala, P. Mittapelly, S. C. Jones, P. M. Piermarini, O. Mittapalli, *Comp. Biochem. Physiol., Part B: Biochem. Mol. Biol.* **2013**, *164*, 275.

[45] D. Heo, E. Lee, M. Ku, S. Hwang, B. Kim, Y. Park, Y. Han Lee, Y. M. Huh, S. Haam, J. H. Cheong, J. Yang, J. S. Suh, *Nanotechnology* **2014**, *25*, 275102.
[46] J. E. Sader, J. W. M. Chon, P. Mulvaney, *Rev. Sci. Instrum.* **1999**, *70*, 3967.
[47] E. K. Dimitriadis, F. Horkay, J. Maresca, B. Kachar, R. S. Chadwick, *Biophys. J.* **2002**, *82*, 2798.
[48] C. Gamonpilas, E. P. Busso, *Mater. Sci. Eng. A* **2004**, *380*, 52.
[49] B. Oommen, K. J. Van Vliet, *Thin Solid Films* **2006**, *513*, 235.
[50] T. K. Berdyyeva, C. D. Woodworth, I. Sokolov, *Phys. Med. Biol.* **2005**, *50*, 81.
[51] T. G. Kuznetsova, M. N. Starodubtseva, N. I. Yegorenkov, S. A. Chizhik, R. I. Zhdanov, *Micron* **2007**, *38*, 824.